CRYSTAL GROWTH & DESIGN

Article

pubs.acs.org/crystal

Continuous Heterogeneous Crystallization on Excipient Surfaces

Nima Yazdanpanah, Christopher J. Testa, Siva R. K. Perala, Keith D. Jensen, Richard D. Braatz, Allan S. Myerson, and Bernhardt L. Trout*

Department of Chemical Engineering, Massachusetts Institute of Technology, Cambridge, Massachusetts 02139, United States
Novartis-MIT Center for Continuous Manufacturing, Cambridge, Massachusetts 02139, United States

Supporting Information

ABSTRACT: A novel continuous heterogeneous crystallization process is developed in which the active pharmaceutical ingredient (API) is crystallized directly on the surface of an excipient within the crystallizer. The product is subsequently dried and formed into tablets without the need for complex downstream processing steps, such as milling, sieving, granulation, and blending. The aim is to eliminate many steps of the particle processing in drug product manufacturing. The APIs and excipients systems were selected by investigating heteroepitaxial mechanisms. The effects of various process parameters, such as temperature, residence time, and mode of operation, on drug loading were studied. Three different process designs—mixed suspension mixed product removal with a traditional impeller, Viscojet mixing, and a fluidized bed crystallizer—were utilized for direct crystallization of the API on the surface of the crystalline excipient. The excipient selection and process design parameters have a significant impact on drug loading, avoidance of bulk nucleation and crystallization, control of API crystal shape and size, and process control. The maximum drug loading of the excipient with API in this study was 47%. Also, it was demonstrated that increasing the supersaturation ratio and residence time increased the drug loading. The products were collected from the crystallizer and directly compressed into tablet form. The tablet hardness and dissolution profile were also studied. The fully continuous process eliminates the downstream steps, resulting in the production of crystalline compounds and the final form (tablets) in a significantly faster, more efficient, and more economical manner with a smaller footprint.

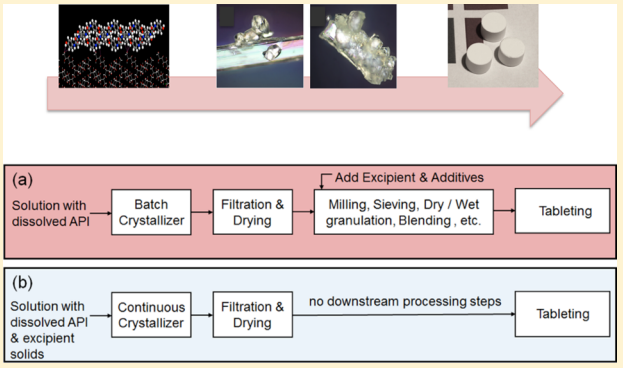

1. INTRODUCTION

The final dosage form for most small-molecule drug products is a spatially uniform mixture of the active pharmaceutical ingredient (API) and excipient(s), which is pressed into tablet form. The downstream process of the drug product manufacturing starts from the crystallization step of the API (drug substance upstream) and often includes many intermediate steps of milling, mixing (with required excipients) and blending, granulation, drying, sieving, and tablet pressing[1−5] (Figure 1a). Many risks, challenges, technical hurdles, and considerations are associated with each of the aforementioned steps.[6−10] The precise final dosage, content uniformity, composition, mechanical properties, and critical quality attribute of every single tablet, which are highly regulated,[2,11−13] highly depend on the performance of the involved stages, for instance, component segregation, which can be caused by differences in particle size, density, or shape, and segregation in blending, hoppers, transfer lines, or feeders, and results in heterogeneity in tablet compositions.[14−17] Significant academic research and industrial development have been invested to overcome drug product line challenges and enable consistent manufacturing of high-quality tablets.[18−22] These challenges, and subsequent effects, are more problematic in the continuous manufacturing arena,[23,24] where the continuous flow of material, continuous workload of the drug product line, residence time distribution, and validation of "batches" of the final product enter into the design of already complicated processes.[17,20,21,23,24]

Recent endeavors in shifting from the traditional batch pharmaceutical processes to the modern and emerging

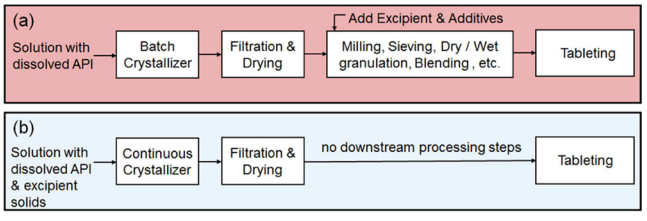

Figure 1. (a) Traditional batch manufacturing of pharmaceuticals. (b) Continuous process utilizing a crystallization step employing heterogeneous nucleation mechanisms.

Received: February 28, 2017
Revised: May 1, 2017
Published: May 16, 2017

DOI: 10.1021/acs.cgd.7b00297
Cryst. Growth Des. 2017, 17, 3321−3330

continuous manufacturing have been toward increasing the efficiency of processing methods in the pharmaceutical industry.[25−27] The ultimate goal of continuous manufacturing is to have an end-to-end integrated process, when economical and logistical considerations make it viable.[25,28] The continuous crystallization of the API is well studied[29−32] and, as of recently, is being more widely implemented in industry. The continuous drug product steps are also well studied and are being adopted by industry rapidly. However, most efforts have been toward improvement of the traditional steps to make them work continuously in a seamless and immaculate sequence.

The techniques introduced in this study represent an avant-garde approach toward eliminating all the intermediate steps of the drug product process and therefore eliminating all the associated challenges. Herein, the API (mixed with excipient) goes directly from the crystallization step to the tablet press with often no need for blending or granulation. In addition, the process is designed in a continuous manner, ready for use in end-to-end integrated continuous manufacturing. The elimination of unneeded unit operations (Figure 1b) also yields significant reductions in the process's footprint and capital and operational costs.

The concept of this work is direct crystallization of an API on a crystalline excipient surface, which is called "heteroepitaxy." The heterosurface orders prenucleation aggregates, so nucleation becomes energetically favorable.[33−35] In the crystallization process detailed here, the API (acetaminophen) nucleates and grows on an excipient surface (D-mannitol). The API−excipient system selection, induction time measurement, and molecular interaction modeling have been studied in previous works of our group,[33,34,36−42] and a theoretical background of the molecular modeling study and excipient selection is described in the Supporting Information. The key criteria in solvent selection are that the solvent has to be able to dissolve the API to make a crystallization solution, but the substrate should have negligible solubility in the solvent. As will be explained later, the amount of API crystal deposition on the surface of the excipient can be easily controlled, which is critical for final dosage control. The composite mixture most often requires no additional blending or further processing and will be uniform and stable during the flow to the tablet press.

All of the previous epitaxy studies of organic molecules have utilized small-scale, stagnant solutions, well-controlled small-vial-size environments, and the batch concept.[34,37,39,43−45] No previous study has reported on employing epitaxy for direct crystallization of an API on an excipient under dynamic conditions, under continuous flow, at pilot scale, or ready for actual industrial application. The dynamic conditions of continuous crystallization and the effects of all transport phenomena and kinetic effects have significant impacts on the process, which are demonstrated and addressed in this study. Continuous crystallization and process stability, spontaneous nucleation (bulk nucleation) at high supersaturation ratio, secondary nucleation and mixing, particle-impeller attrition, and tableting are all addressed. The attrition and fragmentation can be formed by contact of the crystals with a pump impeller, the stirrer blade, or on vessel walls.[46−48] These facts have been the motivation behind this investigation, employing three different mixing mechanisms (a traditional pitch blade impeller, Viscoject, and hydro-fluidization).[49] The effects of crystal−impeller and crystal−crystal collision and attrition on secondary nucleation are further explained in the Supporting Information.

In this study, the novel technique of direct crystallization of an API on the surface of an excipient in a continuous process is introduced. The product is directly compressed into tablets, and all intermediate steps of blend preparation are eliminated. Process properties, challenges, and product quality have been studied for three different process setups. The streamlined concept of the technique and the benefits of minimizing the downstream steps would significantly enable end-to-end integrated continuous manufacturing to be made more efficient and easier to operate.

2. MATERIALS AND METHODS

2.1. Materials. *Chemicals.* Acetaminophen (4-acetamidophenol), metacetamol (3-acetamidophenol), D-mannitol, and sodium chloride with >98% purity were purchased from Sigma-Aldrich. Deionized water was produced from a Barnstead Easypure II (Thermo Scientific) deionizer, and ethanol 200 proof was purchased from VWR International. Materials were used without any further purification. D-Mannitol crystals were processed and conditioned in a cyclic cooling crystallization process to produce large and uniform crystals for the epitaxy process. The reason for selecting acetaminophen, D-mannitol, and sodium chloride will be explained later, and the material selection algorithm is explained in the Supporting Information.

D-Mannitol Crystal Conditioning. As received, the D-mannitol purchased was a fine powder with a wide range of particle sizes (30−150 μm) and shapes, which is the result of the vendor's milling process. The size and shape of the crystals were not suitable for this study due to dusty crystals, which would make bulk nucleation detection difficult, and rough and broken surfaces and edges, which would create challenges in the study of nucleation and the measurement of growth rate. For industrial application and bulk production, perfect shape and size of the excipient crystals may not be essential.

The D-mannitol was aged by temperature cycling to dissolve fine crystals and form uniform crystals with a narrow particle size distribution. The process occurred in a 15-L temperature-controlled well-mixed vessel, where 3 kg of D-mannitol dissolved in a mixture of 2.4 kg of ethanol and 7.8 kg of deionized water. The mixture was held in suspension at 43 °C for 1 h and then was cooled down to 20 °C in a ramp of 1 h and 20 min. The mixture was held at 20 °C for 1 h and then was heated again to 43 °C in a ramp of 1 h and 20 min, and it was held at that temperature for 1 h. The cycle was repeated in this manner until the D-mannitol particles were sufficiently aged and had reached a particle size distribution of 250 to 350 μm. The slurry was then discharged, filtered, washed, and dried in a vacuum oven for 24 h. The dried particles were sieved to remove large agglomerates (more than 350 μm in size) and fine broken particles (smaller than 250 μm), which might be formed during the filtration and drying process. Figure 2 shows D-mannitol crystals after the conditioning process with uniform shape and size. The aging process is a common technique in the crystallization industry; however, the process parameters used here were not standardized, and the procedure was not optimized for a particular particle size distribution or yield.

2.2. Process Setup. *MSMPR.* Figure 3 illustrates the process setup, which was used for the mixed suspension mixed product removal (MSMPR) experiments. The feed vessel was used for batch preparation of a premixed feed solution at certain concentrations (at corresponding temperatures) and suspension densities required for each experiment. Details of the experiments and process conditions are reported in Tables 1 and 2. Supersaturation ratio (ratio of concentration) is designated as $S = C/C^*$, where, S is the supersaturation ratio, C is solution concentration, and C^* is equilibrium concentration (solubility) and corresponding temperature.

Acetaminophen solubility data in ethanol from the literature[50] was used as the basis for feed concentration and feed formulation. The exact amounts of acetaminophen and ethanol (and metacetamol for the purification experiments) were weighed and loaded into the feed vessel to make approximately 5 L of feed solution. The solution was

DOI: 10.1021/acs.cgd.7b00297
Cryst. Growth Des. 2017, 17, 3321−3330

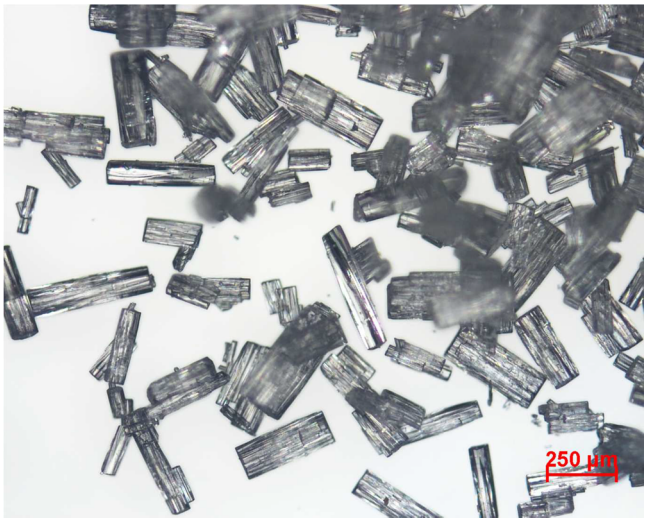

Figure 2. D-Mannitol crystals after the conditioning process with uniform shape and size.

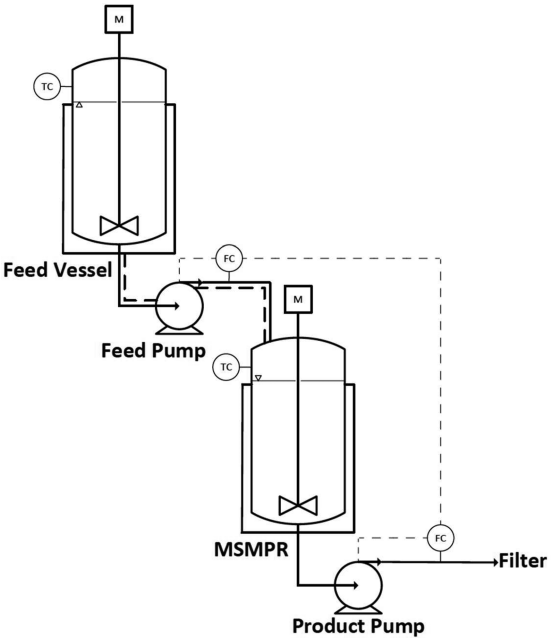

Figure 3. Process flow diagram for the MSMPR experiment with a one-stage crystallizer.

continuously stirred at 180 rpm with an appropriate type and size Viscojet impeller to achieve uniform mixing and dissolve all the solid particles. Then, D-mannitol crystals were added to the feed solution to reach a 4% solution slurry concentration. Solubility of D-mannitol in ethanol is negligible. The slurry was stirred at the adjusted temperature for the entire experiment. A peristaltic pump (Thermo Scientific) was used as the feed dosing pump to continuously transfer the slurry solution from the bottom of the feed vessel via a heat-jacketed line to the top of the MSMPR crystallizer. The flow rate of the feed addition was controlled by the pump speed and synchronized with the product removal pump outflow. The ratio of the volume of the crystallizer, 500 mL, to the flow rate defines the mean residence time for the crystallization process. The feed vessel was located at an elevated height in reference to the feed pump and MSMPR. The product removal pump was also located under the crystallizer vessel with an inlet from the bottom of the vessel. Two types of impellers, a traditional pitch plate and Viscojet cone, were used for the crystallization experiments to study the effects of shear rate, particle-impeller attrition, and secondary nucleation generated by different impeller types (Figure 4). A theoretical background on the impeller selection, particle-impeller attrition and secondary nucleation is described in the Supporting Information. For experiments with multistage MSMPR, the same configuration of the crystallizer, feeding, and product removal were used for the second stage (these results are not reported here; a schematic diagram is included in the Supporting Information). In addition to the online monitoring and measurements, liquid and solid samples were taken every 30 min for off-line analysis during the startup, transition, and steady-state stages. The experiments were continued for at least six residence times before terminating and collecting the final products.

Fluidized Bed Crystallizer. Figure 5 illustrates the process setup used for the crystallization process in a customized continuous fluidized bed crystallizer (CFBC). The feed vessel was used for batch preparation of a premixed feed solution, and the feeding system was the same as the setup used for the MSMPR experiments. The feed solution preparation, condition, and concentration were the same, and the values are reported in Tables 1 and 2. Because of the low turbulence intensity and low shear rate in mixing in the upward flowing column and no particle-impeller collision, fluidized bed crystallizers are very effective in minimizing secondary nucleation.[51,52] The hydrodynamic plug-flow pattern and good mixing at the bottom of the column provide gentle but efficient mixing for sufficient nucleation and growth; however, the advantages cannot be extrapolated for antisolvent applications due to micromixing issues and their effects on crystal size distribution.[53] The high efficiency mixing regime and particle movement are evident in the video clip provided in the Supporting Information.

The custom-made CFBC consists of a double-pipe vessel of 76.2 cm in length and 25 mm in inner diameter, and it is glass-jacketed (Ace Glass Incorporated). A straight funnel-type distributor is used on the bottom of the column for inlet recirculation flow. A diaphragm pump (Solenoid-Diaphragm Metering Pump LMI C921-368SI, Cole Parmer, USA) was placed underneath the column used for the fluidization and flow recirculation. The outlet jet of the diaphragm pump pushes the particles upward through the column, through the funnel distributor, and maintains low-shear well-mixed suspension conditions. The mixing regime and uniformity of the flow can be seen in the video (Supporting Information). A peristaltic pump (Thermo Scientific) was used as the feed dosing pump to continuously transfer the slurry solution from the bottom of the feed vessel via a heat-jacketed line (to prevent cooling and crystallization in the tubing). The feed inlet from the feed vessel enters the suction line of the recirculation pump, which is under slight negative pressure (suction mode), to avoid backflow and clogging. The flow rate of the feed addition was controlled by the pump speed and synchronized with the product removal pump outflow. The recirculation line is outfitted with a FTIR (Thermo Scientific, Nicolet 6700, with a universal immersion probe, Axiom Analytical Incorporated, Dipper-210, operated by Omnic software) that is equipped with a universal immersion probe (Axiom Analytical Incorporated, Dipper-210) operated by Omnic software for in-line monitoring of the concentration using a chemometric model.[54] In addition to the online monitoring and measurements, liquid and solid samples were taken every 30 min for off-line analysis during the startup, transition, and steady-state stages. The experiments were continued for at least six residence times before terminating and collecting the final products.

Startup and Continuous Run Events Profile. Figure 6 shows representative temperature and concentration profiles for startup, transition, and equilibrium (continuous run) statuses of the continuous crystallization system. This particular result is from a selected experiment conducted in the fluidized bed crystallizer, but the events are typical for different types of continuous crystallization, including the MSMPR experiments.

The initial temperature and concentration in the crystallizer (point A), in equilibrium with the feed tank (initial condition), represent the starting point of the profile. The temperature of the solution in the crystallizer ("batch mode" for startup) was then decreased from the feed temperature to the experiment temperature. The drop in

DOI: 10.1021/acs.cgd.7b00297
Cryst. Growth Des. 2017, 17, 3321−3330

Table 1. Experimental Conditions and Results for Continuous Crystallization with 30 min Residence Time by Three Different Mixing Tools

method	rpm	feed T (°C)	exp T (°C)	initial supersaturation ratio	steady-state supersaturation ratio	residence time (min)	drug loading (wt %) (g drug/g total solid)
fluidized bed		20	10	1.21	1.030	30	18.5
fluidized bed		27	10	1.40	1.033	30	27.0
fluidized bed		33	10	1.58	1.046	30	41.9
fluidized bed		35	10	1.64	1.053	30	47.0
fluidized bed		38	10	1.74	1.060	30	BN[a]
impeller	200	20	10	1.21	1.030	30	18.3
impeller	200	25	10	1.34	1.032	30	24.1
impeller	200	27	10	1.40	1.035	30	28.7
impeller	200	30	10	1.49	1.041	30	BN
Viscojet	220	20	10	1.21	1.030	30	18.5
Viscojet	220	25	10	1.34	1.032	30	24.0
Viscojet	220	27	10	1.40	1.033	30	28.0
Viscojet	220	30	10	1.49	1.041	30	35.0
Viscojet	220	33	10	1.58	1.046	30	41.8
Viscojet	220	35	10	1.64	1.053	30	BN

[a]BN: bulk (spontaneous) nucleation.

Table 2. Experimental Conditions and Results for Continuous Crystallization with 45 min Residence Time by Three Different Mixing Tools

method	rpm	feed T (°C)	exp T (°C)	initial supersaturation ratio	steady-state supersaturation ratio	residence time (min)	drug loading (wt %) (g drug/g total solid)
fluidized bed		20	10	1.21	1.020	45	21.2
fluidized bed		27	10	1.40	1.027	45	32.0
fluidized bed		30	10	1.49	1.037	45	41.0
fluidized bed		33	10	1.58	1.041	45	44.1
fluidized bed		38	10	1.74	1.060	45	BN[a]
impeller	200	20	10	1.21	1.021	45	21.0
impeller	200	25	10	1.34	1.023	45	28.2
impeller	200	27	10	1.40	1.028	45	33.5
impeller	200	30	10	1.49	1.041	45	BN
Viscojet	220	20	10	1.21	1.020	45	21.2
Viscojet	220	25	10	1.34	1.023	45	27.3
Viscojet	220	27	10	1.40	1.027	45	32.0
Viscojet	220	30	10	1.49	1.037	45	40.7
Viscojet	220	33	10	1.58	1.041	45	44.5
Viscojet	220	35	10	1.64	1.053	45	BN

[a]BN: Bulk (spontaneous) nucleation.

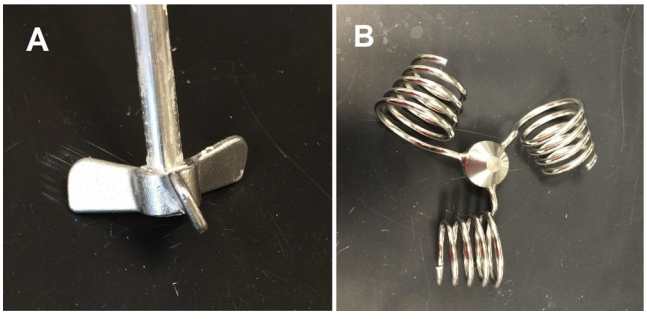

Figure 4. Two types of impellers used in this study: (A) a traditional pitch blade impeller and (B) a basket-shaped coil Viscojet.

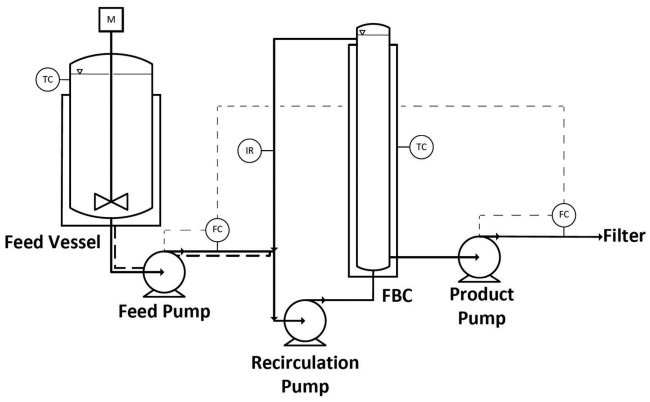

Figure 5. Process flow diagram for the experiments with the fluidized bed crystallizer.

temperature initiates nucleation, which is represented by a delay (response to the event) in the concentration profile (period A–B). Period B–C corresponds to the crystal growth phase until the system reached the concentration equilibrium at the corresponding supersaturation ratio and solubility. The concentration difference (solubility difference) between the initial condition (feed tank) and the crystallizer is referred to as the initial supersaturation ratio in Tables 1 and 2. The solution stays at the equilibrium condition for a few hours to ensure steady-state conditions before the start (point D) of

DOI: 10.1021/acs.cgd.7b00297
Cryst. Growth Des. 2017, 17, 3321–3330

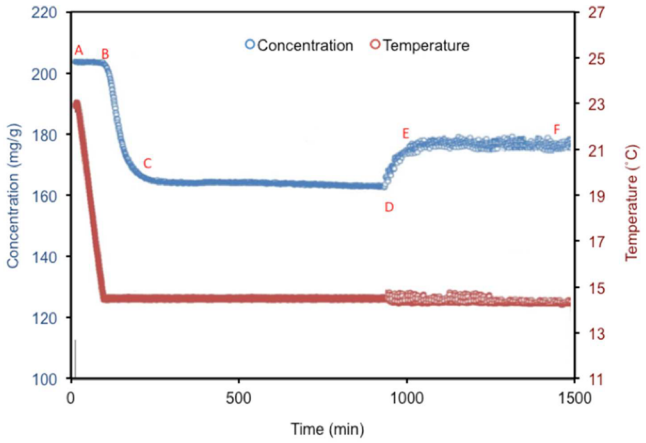

Figure 6. Temperature and concentration profiles for the preflow start-up (batch) (A–D), transition (D–E), continuous (D–F), and steady-state stages (C–D, E–F).

the continuous experiments (starting the feed pump and product pump). The pumps' drives and flow rates are synchronized based on the required residence time in the crystallizers. While the temperature remains constant at the crystallizer, there is an obvious transition period in the concentration profile (period D–E). The negligible fluctuation in the temperature is due to the cooler duty and dynamic adjustment of temperature caused by the addition of the warmer inlet solution. The transition period comprises a short period of time before the system reaches steady-state. The process is considered to be at steady-state conditions after 4–6 residence times (period E–F). The concentration difference between the steady-state condition and solubility at the corresponding temperature is referred to as the steady-state supersaturation ratio in Tables 1 and 2. The temperature and concentration of the solution were measured by in-line probes, and solid and solution samples were taken during the experiments for at-line analysis for confirmation of the concentration, image analysis of crystals (excipients and API), and monitoring of bulk nucleation. At the end of the experiments (point F), the powders were collected over a vacuum filter for further analysis of the product and to make tablets.

2.3. Analytical Methods and PAT. The melting point depression and solid interaction were analyzed by modulated differential scanning calorimetry (MDSC). MDSC samples were prepared according to standard procedures using aluminum hermetically sealed pans. Three samples of each material were analyzed to check the repeatability of the results. The samples were heated from 0 to 200 °C using a ramp rate of 5 °C/min with a 1 °C modulated signal every 60 s using a modulated differential scanning calorimeter (TA Instruments Q1000, DE, USA).

Powder X-ray diffraction (PXRD) analysis was performed on the solid product using an X' Pert PRO XRD PANanalytical at 45 kV, 40 mA beam energy for the range of 2θ = 4–40° at a resolution of 0.0418°/s).

Solid products were also analyzed by Raman spectroscopy (RXN1-785, Kaiser Optical Systems Inc.) with settings of λ = 785 nm and max power rating = 450 mW.

Optical microscope images of the solid product were taken to qualitatively assess the degree of primary and secondary nucleation with an Olympus BX51 microscope and Infinity Analyze software Revision 5.0.3.

The particle size distributions of D-mannitol crystals and final products were measured by laser diffraction particle sizing using a Malvern Mastersizer 2000 (Malvern Instruments, UK).

The online Fourier transform infrared (FTIR) spectrometer was used for continuous online monitoring and recording of the crystallization process. The amount of acetaminophen on the D-mannitol surfaces (drug loading) was determined with the density meter. The density of liquid samples was measured using an Anton Paar DMA 4100 M density meter. A calibration model relating density and the temperature set on the density meter to concentration was used to determine the concentration of the liquid samples. The solid samples were dried in a vacuum oven, and then a known quantity was added to a known quantity of ethanol and allowed to sit in a heated sonicated water bath for approximately an hour and a half, allowing the acetaminophen to dissolve. The solution was then filtered and analyzed on the density meter.

The purity of the final samples (for purification experiments) was tested with an HPLC instrument (Agilent 1100) equipped with a UV diode array detector. The column used was a YMC-Pack ODS-A 150 mm × 4.6 mm i.d. column packed with 3-μm particles with 12 nm pore size (YMC America Inc.). The detection wavelength was set at 254 nm for acetaminophen and 230 nm for metacetamol. The samples were analyzed using an isocratic method with a 30:70 methanol/water mobile phase containing 0.3% trifluoroacetic acid for 10 min.

Solid-state samples were directly compressed into tablets of different weights (70–150 mg) using a 6 mm die with compaction pressures of 170 and 475 kg using a Gamlen tablet press (GTP-1) controlled by GTP1 Controller/Graph Plotter, v. 3.21.

Tablet strength was tested with a Dr. Schleuniger Pharmatron model 6D Tablet Tester.

The control system included a computer setup (Dell, Optiplex 745) with LabView 2012 software, which receives and sends data using a data acquisition system, an NI CompactDAQ chassis (National Instruments, NI cDAQ-9178) equipped with various signal modules, and RTD's and thermocouples for temperature control and system monitoring, respectively.

The method to test the dissolution of the tablets was based on the USP monograph for acetaminophen tablets. It was performed using a USP apparatus II (paddle) on an Agilent 708-DS dissolution tester equipped with a Cary 50 fiber optic UV detector (Agilent Technologies, Santa Clara, CA). The dissolution medium used was a phosphate buffer at a pH of 5.8, and the media temperature was maintained at 37.0 ± 0.5 °C. These conditions were chosen as per the USP chapter 711 specifications for the dissolution of acetaminophen tablets.

3. RESULTS AND DISCUSSION

3.1. Continuous Runs, Drug Loading, and Bulk Nucleation. Continuous crystallization experiments were performed for different supersaturation ratios, residence times, and types of mixing (traditional pitched blade impeller, Viscojet, and Fluidized Bed). Tables 1 and 2 report the experimental results for the three categories at two residence times of 30 and 45 min (a total of six sets of experiments). All the continuous crystallization experiments were performed at 10 °C, and the increase of the supersaturation ratio was achieved by increasing the feed concentration (and temperature), which is reported as the initial supersaturation ratio (concentration difference at the corresponding feed temperature and crystallizer temperature). The drug loading is determined as the amount of acetaminophen on the D-mannitol surfaces, which improves with an increase of the supersaturation ratio and residence time. The maximum drug loading is defined at the highest supersaturation ratio for which bulk nucleation (spontaneous nucleation) occurs in the solution. At that maximum level, small acetaminophen crystals are formed in the solution and are separate from the D-mannitol. However, the total amount of the acetaminophen content in the product is higher (sum of the content both off and on the excipient surface) due to crystallization from the higher-supersaturated solution, but that condition is unacceptable for the purpose of this study. For instance, for an initial supersaturation ratio of 1.2 and residence time of 30 min, the average drug loading for the products from experiments with the fluidized bed, impeller, or Viscojet is 18.5 wt % (g drug/g total solid).

DOI: 10.1021/acs.cgd.7b00297
Cryst. Growth Des. 2017, 17, 3321–3330

The maximum achieved drug loading at the maximum supersaturation ratio for the experiments with the impeller is 28.7 wt %, for Viscojet is 41.8 wt %, and for the fluidized bed is 47 wt %. Further increasing the supersaturation ratio causes spontaneous nucleation, which is marked as failed experiments here (BN at Tables 1 and 2 = bulk nucleation). As described in the Supporting Information, the difference in hydrodynamic effect, particle-impeller attrition, and shear rate by different mixing causes less secondary and bulk nucleation, and therefore the drug loading can be higher for the most gentle mixing. Because of the low turbulence intensity and low shear rate in mixing in the upward flowing column and the lack of particle-impeller collisions, fluidized bed crystallizers are very effective in minimizing secondary nucleation. This result demonstrates that the highest loading occurs for the fluidized bed, then Viscojet, and finally the impeller.

The experiments of this study are under dynamic and well-mixed conditions, where the hydrodynamic effect of mixing provides sufficient mass transfer; therefore, the nucleation induction time is significantly shorter. In contrast, under static conditions, the nucleation induction time of acetaminophen on D-mannitol was measured as 390 min and reported in Table S1 and in the literature.[34] The experiments for measuring the nucleation induction time were performed in small vials and under stagnant conditions.

The drug loading can easily be tuned by changing the residence time and supersaturation ratio—lowering the residence time and/or supersaturation ratio decreases the drug loading. For example, increasing the residence time from 30 to 45 min increased the drug loading from 29 to 34 wt % for the experiments with a fluidized bed at an initial supersaturation ratio of 1.4. The steady-state supersaturation ratio also decreased from 1.033 for the residence time of 30 min to 1.027 for the 45 min experiment, which shows that molecules had more time to incorporate into crystals and precipitate on the surface of the excipient. Within equipment limitations, a longer residence time can be achieved by increasing the size of the crystallization vessel and/or lowering inlet/outlet flow rate.

Figure 7 shows two samples of experiments with the CFBC at different supersaturation ratios. Figure 7A is for the

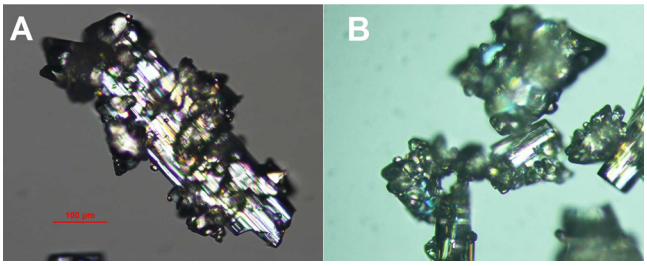

Figure 7. Two samples of experiments with the fluidized bed at a supersaturation ratio of (A) 1.4 and (B) 1.64.

experiment at a supersaturation of 1.4, and Figure 7B is for the experiment at 1.64, and both have a residence time of 30 min. The D-mannitol crystals in Figure 7B are fully loaded with acetaminophen crystals. This sample was from the maximum drug loading achieved by these series of experiments. In addition to the spontaneous nucleation, increasing the supersaturation ratio stacks more crystals (larger group of crystals) on the surface of D-mannitol and increases the chance of breakage and removal of the agglomerates from the surface of the excipient (which is called excipient "baldness").

The particle sizes of the final products were measured by laser diffraction particle sizing and compared with raw materials. Figure 8 shows the particle size distribution for

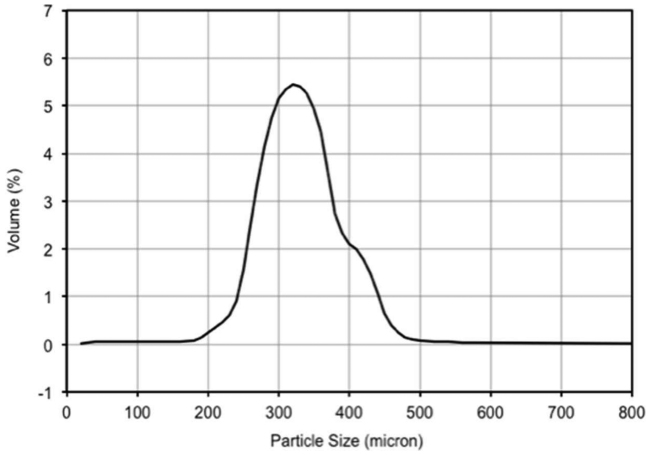

Figure 8. Particle size distribution for products with 34% drug loading.

products with 34 wt % drug loading, which were harvested from the experiment with the fluidized bed with a 45 min residence time and initial supersaturation ratio of 1.4. The raw excipient had been sieved, and a cut of 250−350 μm was used for the experiment. The laser diffraction particle sizing results shows two small shoulders approximately 200 and 400 μm, which could be related to particle breakage or agglomeration during filtration and drying. The laser diffraction particle sizing (1D) is not a proper technique for this type of high aspect ratio crystal, where the size increase would be in the width of the crystals. A combination of image analysis and laser diffraction would better serve the purpose and is recommended for further study.[55]

3.2. Purification. The process of capturing impurities in crystals during their growth from the liquid phase could be affected by several factors,[56] including the equilibrium distribution coefficient (matrix inclusion), impurities from solvent inclusion (solvent pockets formed in crystals), and/or entrapment of impurities between crystals. The purification performance of the continuous crystallization on the surface of the excipient was investigated via a few experiments to demonstrate the effectiveness of the technique in rejecting impurities as well. A few of the previous experiments with Viscojet with a 45 min residence time and different levels of supersaturation ratio were repeated with the presence of 5 wt % of impurity (metacetamol) in the solution. Metacetamol is one of the main structurally related impurities for the acetaminophen and has a high tendency for being incorporated in the crystal matrix; its equilibrium distribution coefficient (under ideal crystallization conditions) was presented before.[57]

Table 3 presents results for the purification experiments with 5 wt % starting amount of impurity. The maximum final purity is 98.4 wt % (g acetaminophen/(g acetaminophen + g metacetamol)) and is achieved at a lower supersaturation ratio, where the crystal growth rate is slower. In contrast, the lowest purity achieved from the high supersaturation ratio of 1.49 was 98 wt % by starting the solution purity at 95 wt %. The comparison of drug loading and steady-state supersaturation ratio in Table 3 and the matching experiments in Table 2 show that the average drug loading for similar

DOI: 10.1021/acs.cgd.7b00297
Cryst. Growth Des. 2017, 17, 3321−3330

Table 3. Purification Results from Experiments with 5 wt % Initial Impurity, Performed at Different Supersaturation Ratios, with Viscojet with a 45 min Residence Time

method	rpm	feed T (°C)	exp T (°C)	initial supersat ratio	steady-state supersat ratio	residence time (min)	drug loading[a] (wt %)	purity[b] (wt %)	dist coef[c]
Viscojet	220	25	10	1.34	1.027	45	26.1	98.4	0.32
Viscojet	220	27	10	1.4	1.031	45	31	98.3	0.34
Viscojet	220	30	10	1.49	1.041	45	40	98	0.40

[a]Drug loading here: (g acetaminophen + g metacetamol)/g total solid (acetaminophen + metacetamol + D-mannitol). [b]Purity: g acetaminophen/(g acetaminophen + g metacetamol). [c]Effective distribution coefficient $= \frac{(C_{imp}/C_H)_{solid}}{(C_{imp}/C_H)_{liquid}}$

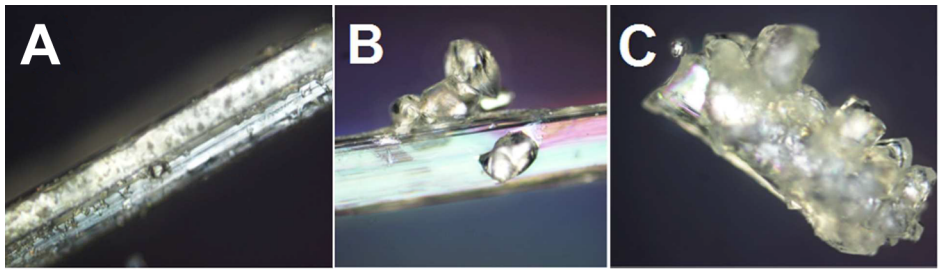

Figure 9. (A–C) Different sizes of acetaminophen crystals on the surface of D-mannitol under different growth conditions (supersaturation and time).

experiments is lower in the presence of the impurity than in the pure solution and that the steady-state supersaturation ratio is higher in the presence of the impurity. The cause of this phenomenon is the effect of metacetamol in increasing the solubility of acetaminophen, which has been investigated before.[57]

3.3. Growth Rate Measurement and Calculation. Despite the various techniques and instruments developed for in-line and off-line crystal size measurement and growth rate monitoring, measuring the crystallization rate based on the size and number of crystals was very challenging for such composite excipient–API crystals. The existence of excipient crystals in the slurry causes significant noise in Focused Beam Reflectance Measurement (FBRM) measurements, to the extent that the measured chord length distributions are not quantitative.

Figure 9 shows different stages of acetaminophen crystal nucleation and growth on the surface of D-mannitol excipient crystals, in which the samples were taken from continuous experiments and analyzed off-line. Figure 9A shows the "first stage" of nucleation, during which small structures appeared on the surface of the excipient. Figure 9B shows a sample from a different experiment (at a lower supersaturation), where a few crystals are grown on the surface of the excipient. Figure 9C shows a sample from another experiment (at higher supersaturation), where a group of crystals are grown on the surface of the excipient.

Image analysis techniques could potentially be used to measure the growth rate by collecting hundreds of images in a short period of time, subtracting the D-mannitol domain from the images, and compiling the average size and number of crystals. However, as is obvious from the images, the crystals do not appear at the same location on the D-mannitol surface; some crystals are out of the focal point, and blurred edges would cause an error in reading the size via image analysis software. Additionally, different sizes of crystals form a group of crystals, which makes the differentiation task difficult for image analysis software. The domain heterogeneity and size distribution of the group of crystals need to be addressed in future measurement attempts, for instance, by robust and advanced imaging or image analysis techniques.

To estimate the growth rate under different process conditions, population balance and de-supersaturation modeling were applied to batch experiments, which provides a rough estimate of the process performance. The method and results can be found in the Supporting Information.

3.4. Effects of Different Excipients (D-Mannitol vs. Sodium Chloride). Heterogeneous nucleation by definition can occur on any foreign particle, such as dust, which is the distinction between homogeneous and heterogeneous nucleation. The presence of excipient crystals in the crystallization solution enhances the nucleation and yields the epitaxy. As mentioned previously, the difference in excipient selection is based on the matching ranking matrix, which is driven from molecular dynamic modeling and induction time measurement experiments. Table S1 (Supporting Information) shows that D-mannitol is the best candidate for acetaminophen crystallization and that sodium chloride is the worst excipient among the studied excipients (D-mannitol, alpha lactose monohydrate, and sodium chloride). The induction time (a in stagnant solution) for D-mannitol was measured as 390 min versus 905 min for sodium chloride. In dynamic conditions where the well-mixed environment provides sufficient mass transfer and molecular flux, the measured static nucleation induction time plays a less important role. The continuous flow, continuous crystallization, hydrodynamic effects, and transition from the start time to steady-state condition significantly affects the nucleation rate (versus the nucleation induction time under stagnant conditions).

Figure 10 shows microscope images of two experiments with sodium chloride as the excipient. The experiments were performed under conditions similar to the previous D-mannitol cases with Viscoject with a 45 min residence time. The first experiment (Figure 10A) was at the supersaturation ratio of 1.2, and the result is very similar to the D-mannitol case. No bulk nucleation is evident, the drug loading was similar (21 wt %), and group of crystals of the acetaminophen crystals have very similar packing (individual crystal size versus agglomerate size).

DOI: 10.1021/acs.cgd.7b00297
Cryst. Growth Des. 2017, 17, 3321–3330

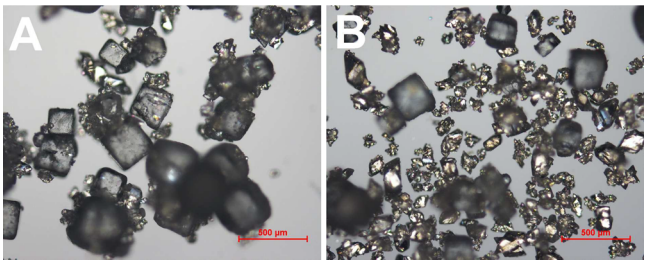

Figure 10. Continuous crystallization experiments for direct crystallization of acetaminophen on the surface of sodium chloride crystals at supersaturation ratios of (A) 1.2 and (B) 1.4.

The experiment at a higher (medium) supersaturation ratio yielded drastically different results than the similar D-mannitol case. Figure 10B shows the products from an experiment performed at a supersaturation ratio of 1.4. No acetaminophen crystals precipitated on the surface of the sodium chloride crystals; instead, they all formed individually in bulk, most likely from spontaneous nucleation, or around dusty size particulate matters in the solution. In contrast, D-mannitol had no crystal segregation at the supersaturation ratio of 1.4, which could also be further increased to 1.58 (in the experiment with Viscojet with a 45 min residence time).

3.5. Tablet Production and Tablet Properties. Harvested crystals from the crystallizer were dried and directly compressed into tablets without any further processing steps (Figure 11). The equipment and process were described in the

Figure 11. Tablets prepared by direct compression of harvested crystals directly from the crystallizer without further processing (blending, granulation, etc.).

Materials and Methods. Two setups were used for the pressure and the number of presses. The tablet hardness was then measured. The tablets prepared under 170 kg of force with a single press had very low strength. Increasing the compression force to 475 kg had a significant effect on the hardness of the tablets and improved the strength by 2-fold (Table 4). The relatively low tablet hardness could be due to three major factors. The powders were directly pressed, and no binder was used. In general, rod-shaped excipient crystals provide low packing efficiency, and tablets that are prepared from needle-shaped crystals (such as carbamazepine form II) have very low mechanical strength.[58,59] Acetaminophen crystals have a low tendency for binding to each other and forming strong bridges under tableting pressure.[58,60] For the latter reason, higher tablet hardness will be expected for other APIs, for instance, aspirin. To overcome the overall challenge, employing different excipients would provide increased tablet hardness. For instance, lactose is one of the preferable excipients for direct crystallization of acetaminophen, which can be substituted by D-mannitol. Lactose is a strong binder that can strengthen the matrix integrity. In addition, the alpha-lactose crystal has a tomahawk shape, which provides better particle packing in the tablet matrix. Excipients can be added to the collection stream as we previously demonstrated,[25] or if they are insoluble, they can potentially be added to the feed or crystallization vessels.

Table 4. Tablet Press Parameters and Tablet Properties

method	tablet weight (mg)	tablet hardness (MPa)
170 kg, single press	93	0.6
475 kg, 3 presses	107	1.4

The prepared tablets were subjected to USP dissolution tests to compare the release behavior of the API. All tablets tested had the same mass and were prepared using the same pressure, meaning that the surface area, volume, and hardness were very similar. However, as the tablet strength tests show, the tablets are relatively weak and disintegrate easily upon contact with the solvent. Figure 12 shows the dissolution profile for the prepared

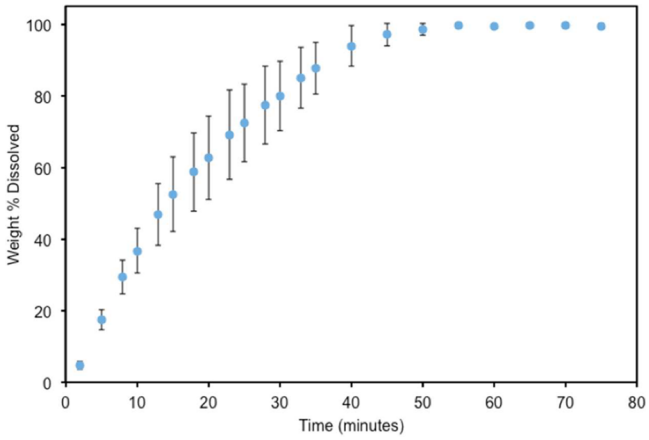

Figure 12. Dissolution profile.

tablets. The release profile shows that 80% of the acetaminophen was dissolved in 30 min. The release profile could be slowed by making harder tablets with the help of the aforementioned strategies.

4. CONCLUSIONS

A novel continuous heterogeneous crystallization concept in which the API was crystallized directly on the surface of an excipient within the crystallizer was investigated. The continuous processes were run via three different methods: a MSMPR with a traditional pitched blade impeller, a coiled Viscojet agitator, and a fluidized bed crystallizer. The aim was to eliminate many of the steps of the particle processing in drug product manufacturing. The fully continuous processes that eliminate the downstream steps results in the production of crystalline compounds and the final form (tablets) in a manner that has a lower footprint and is significantly faster, more efficient, and more economical.

The effects of various process parameters, such as temperature, residence time, and mode of operation, on drug loading and spontaneous nucleation were studied. The drug loading is easily tunable by changing the supersaturation ratio and residence time. The maximum achievable level of drug loading was under the condition in which no bulk nucleation occurs,

DOI: 10.1021/acs.cgd.7b00297
Cryst. Growth Des. 2017, 17, 3321−3330

and all of the crystallization occurs on the surface of the excipient. Different hydrodynamic effects, particle-impeller attrition, and shear rates by different mixing resulted in less secondary and bulk nucleation. Therefore, the highest loading was observed for the fluidized bed, the Viscojet, and finally the traditional pitched blade impeller. For the crystallization of acetaminophen on D-mannitol, the maximum loading in this study was 47 wt %, which was from the experiments in a CFBD with a feed supersaturation ratio of 1.64 and residence time of 30 min. Although higher residence time could yield higher drug loading, increasing the supersaturation ratio caused spontaneous nucleation.

The purification performance of the technique was investigated by the presence of 5 wt % of impurity (metacetamol) in the solution. The results show that purification depends on the supersaturation ratio and crystal growth rate. The maximum final purity was 98.4 wt %, which was achieved at a lower supersaturation ratio.

The powder products were directly compressed in a tablet press at different compaction pressures. The tablets had a nice shape and appearance. The tablet hardness test results indicate that the strength of the tablets is in the low category, which might be an issue in a friability test and dissolution (fast disintegration). Various strategies were suggested to improve the strength of the tablets.

■ ASSOCIATED CONTENT

Supporting Information

The Supporting Information is available free of charge on the ACS Publications website at DOI: 10.1021/acs.cgd.7b00297.

Heteroepitaxial nucleation, crystal-impeller collision and secondary nucleation, growth rate modeling, solid state analysis (PDF)

Movie clip of mixing in fluidized bed (AVI)

■ AUTHOR INFORMATION

Corresponding Author

*E-mail: trout@mit.edu.

ORCID

Nima Yazdanpanah: 0000-0001-7400-1266

Allan S. Myerson: 0000-0002-7468-8093

Bernhardt L. Trout: 0000-0003-1417-9470

Notes

The authors declare no competing financial interest.

■ ACKNOWLEDGMENTS

We would like to acknowledge Novartis International AG for its generous funding of this research.

■ REFERENCES

(1) Dürig, T., Binders in Pharmaceutical Granulation. In *Handbook of Pharmaceutical Granulation Technology*, 3rd ed.; CRC Press, 2009; pp 78−97.

(2) Yu, L. X. Pharmaceutical Quality by Design: Product and Process Development, Understanding, and Control. *Pharm. Res.* **2008**, *25* (4), 781−791.

(3) Hausman, D. S. Comparison of Low Shear, High Shear, and Fluid Bed Granulation During Low Dose Tablet Process Development. *Drug Dev. Ind. Pharm.* **2004**, *30* (3), 259−266.

(4) Faure, A.; York, P.; Rowe, R. C. Process control and scale-up of pharmaceutical wet granulation processes: a review. *Eur. J. Pharm. Biopharm.* **2001**, *52* (3), 269−277.

(5) Armstrong, N. A. Tablet manufacture by direct compression. *Encyclopedia of Pharmaceutical Technology*, 3rd ed.; Swarbrick, J., Ed.; Informa Healthcare: New York, 2007; Vol. *1*, pp 3673−83.

(6) Andrews, G.; Jones, D.; Zhai, H.; Diak, O. A.; Walker, G., Effects of Grinding in Pharmaceutical Tablet Production. In *Pharmaceutical Manufacturing Handbook*; John Wiley & Sons, Inc., 2007; pp 1165−1190.

(7) Picker-Freyer, K. M., Tablet Production Systems. In *Pharmaceutical Manufacturing Handbook*; John Wiley & Sons, Inc., 2007; pp 1053−1098.

(8) Huang, J.; Kaul, G.; Cai, C.; Chatlapalli, R.; Hernandez-Abad, P.; Ghosh, K.; Nagi, A. Quality by design case study: An integrated multivariate approach to drug product and process development. *Int. J. Pharm.* **2009**, *382* (1−2), 23−32.

(9) Vaithiyalingam, S. R.; Sayeed, V. A. Critical factors in manufacturing multi-layer tablets—Assessing material attributes, in-process controls, manufacturing process and product performance. *Int. J. Pharm.* **2010**, *398* (1−2), 9−13.

(10) Bogda, M. J. Tablet compression: Machine theory, design, and process troubleshooting. *Encyclopedia of Pharmaceutical Technology*; Swarbrick, J., Ed.; Informa Healthcare: New York, 2007; p 3614.

(11) Ahuja, S.; Scypinski, S. *Handbook of Modern Pharmaceutical Analysis*; Academic Press, 2010; Vol. *10*.

(12) Gowen, A.; O'donnell, C.; Cullen, P. J.; Bell, S. Recent applications of chemical imaging to pharmaceutical process monitoring and quality control. *Eur. J. Pharm. Biopharm.* **2008**, *69* (1), 10−22.

(13) Lawrence, X. Y.; Akseli, I.; Allen, B.; Amidon, G.; Bizjak, T. G.; Boam, A.; Caulk, M.; Doleski, D.; Famulare, J.; Fisher, A. C. Advancing product quality: a summary of the second FDA/PQRI conference. *AAPS J.* **2016**, *18* (2), 528−543.

(14) Karmarkar, S.; Garber, R.; Genchanok, Y.; George, S.; Yang, X.; Hammond, R. Quality by Design (QbD) Based Development of a Stability Indicating HPLC Method for Drug and Impurities. *J. Chromatogr. Sci.* **2011**, *49* (6), 439−446.

(15) Ermer, J.; Miller, J. H. M. *Method Validation in Pharmaceutical Analysis: a Guide to Best Practice*; John Wiley & Sons, 2006.

(16) Moes, J. J.; Ruijken, M. M.; Gout, E.; Frijlink, H. W.; Ugwoke, M. I. Application of process analytical technology in tablet process development using NIR spectroscopy: Blend uniformity, content uniformity and coating thickness measurements. *Int. J. Pharm.* **2008**, *357* (1), 108−118.

(17) Shi, Z.; McGhehey, K. C.; Leavesley, I. M.; Manley, L. F. On-line monitoring of blend uniformity in continuous drug product manufacturing process—the impact of powder flow rate and the choice of spectrometer: dispersive vs. FT. *J. Pharm. Biomed. Anal.* **2016**, *118*, 259−266.

(18) Mitra, B.; Hilden, J.; Litster, J. D. Novel use of monodisperse granules to deconvolute impacts of granule size versus granule solid fraction on tablet tensile strength. *Adv. Powder Technol.* **2015**, *26* (2), 553−562.

(19) Mitra, B.; Hilden, J.; Litster, J. D. Compaction mechanics of plastically deformable dry granules. *Powder Technol.* **2016**, *291*, 328−336.

(20) Singh, R.; Velazquez, C.; Sahay, A.; Karry, K. M.; Muzzio, F. J.; Ierapetritou, M. G.; Ramachandran, R. Advanced control of continuous pharmaceutical tablet manufacturing processes. *Process Simulation and Data Modeling in Solid Oral Drug Development and Manufacture* **2016**, 191−224.

(21) Järvinen, M. A.; Paaso, J.; Paavola, M.; Leiviskä, K.; Juuti, M.; Muzzio, F.; Järvinen, K. Continuous direct tablet compression: effects of impeller rotation rate, total feed rate and drug content on the tablet properties and drug release. *Drug Dev. Ind. Pharm.* **2013**, *39* (11), 1802−1808.

(22) Rehrl, J.; Gruber, A.; Khinast, J. G.; Horn, M. Sensitivity analysis of a pharmaceutical tablet production process from the control engineering perspective. *Int. J. Pharm.* **2017**, *517* (1), 373−382.

(23) Wahl, P.; Pucher, I.; Scheibelhofer, O.; Kerschhaggl, M.; Sacher, S.; Khinast, J. Continuous monitoring of API content, API distribution

and crushing strength after tableting via near-infrared chemical imaging. *Int. J. Pharm.* **2017**, *518* (1), 130−137.
(24) Pawar, P.; Wang, Y.; Keyvan, G.; Callegari, G.; Cuitino, A.; Muzzio, F. Enabling real time release testing by NIR prediction of dissolution of tablets made by continuous direct compression (CDC). *Int. J. Pharm.* **2016**, *512* (1), 96−107.
(25) Mascia, S.; Heider, P. L.; Zhang, H.; Lakerveld, R.; Benyahia, B.; Barton, P. I.; Braatz, R. D.; Cooney, C. L.; Evans, J. M. B.; Jamison, T. F.; Jensen, K. F.; Myerson, A. S.; Trout, B. L. End-to-End Continuous Manufacturing of Pharmaceuticals: Integrated Synthesis, Purification, and Final Dosage Formation. *Angew. Chem., Int. Ed.* **2013**, *52* (47), 12359−12363.
(26) McGlone, T.; Briggs, N. E. B.; Clark, C. A.; Brown, C. J.; Sefcik, J.; Florence, A. J. Oscillatory Flow Reactors (OFRs) for Continuous Manufacturing and Crystallization. *Org. Process Res. Dev.* **2015**, *19* (9), 1186−1202.
(27) Yazdanpanah, N. Continuous Manufacturing of Pharmaceutical and Biopharmaceutical Agents. *Producing More with Less In High Value Processing Technologies*; Aydin Berenjian, H. J. M., Yuanda, S., Ed.; Nova Science Publisher, New York, USA, 2016.
(28) Schaber, S. D.; Gerogiorgis, D. I.; Ramachandran, R.; Evans, J. M. B.; Barton, P. I.; Trout, B. L. Economic Analysis of Integrated Continuous and Batch Pharmaceutical Manufacturing: A Case Study. *Ind. Eng. Chem. Res.* **2011**, *50* (17), 10083−10092.
(29) Lawton, S.; Steele, G.; Shering, P.; Zhao, L.; Laird, I.; Ni, X.-W. Continuous Crystallization of Pharmaceuticals Using a Continuous Oscillatory Baffled Crystallizer. *Org. Process Res. Dev.* **2009**, *13* (6), 1357−1363.
(30) Quon, J. L.; Zhang, H.; Alvarez, A.; Evans, J.; Myerson, A. S.; Trout, B. L. Continuous Crystallization of Aliskiren Hemifumarate. *Cryst. Growth Des.* **2012**, *12* (6), 3036−3044.
(31) Wong, S. Y.; Tatusko, A. P.; Trout, B. L.; Myerson, A. S. Development of Continuous Crystallization Processes Using a Single-Stage Mixed-Suspension, Mixed-Product Removal Crystallizer with Recycle. *Cryst. Growth Des.* **2012**, *12* (11), 5701−5707.
(32) Ferguson, S.; Ortner, F.; Quon, J.; Peeva, L.; Livingston, A.; Trout, B. L.; Myerson, A. S. Use of Continuous MSMPR Crystallization with Integrated Nanofiltration Membrane Recycle for Enhanced Yield and Purity in API Crystallization. *Cryst. Growth Des.* **2014**, *14* (2), 617−627.
(33) Chadwick, K.; Myerson, A.; Trout, B. Polymorphic control by heterogeneous nucleation-A new method for selecting crystalline substrates. *CrystEngComm* **2011**, *13* (22), 6625−6627.
(34) Chadwick, K.; Chen, J.; Myerson, A. S.; Trout, B. L. Toward the Rational Design of Crystalline Surfaces for Heteroepitaxy: Role of Molecular Functionality. *Cryst. Growth Des.* **2012**, *12* (3), 1159−1166.
(35) Ward, M. D. Bulk crystals to surfaces: Combining X-ray diffraction and atomic force microscopy to probe the structure and formation of crystal interfaces. *Chem. Rev.* **2001**, *101*, 1697−1725.
(36) Diao, Y.; Myerson, A. S.; Hatton, T. A.; Trout, B. L. Surface Design for Controlled Crystallization: The Role of Surface Chemistry and Nanoscale Pores in Heterogeneous Nucleation. *Langmuir* **2011**, *27* (9), 5324−5334.
(37) Chadwick, K.; Trout, B. L.; Myerson, A. S. Methods and systems relating to the selection of substrates comprising crystalline templates for the controlled crystallization of molecular species. US20130118399A1, May 16, 2013, *2013*.
(38) Quon, J. L.; Chadwick, K.; Wood, G. P. F.; Sheu, I.; Brettmann, B. K.; Myerson, A. S.; Trout, B. L. Templated Nucleation of Acetaminophen on Spherical Excipient Agglomerates. *Langmuir* **2013**, *29* (10), 3292−3300.
(39) Chunsrivirot, S.; Diao, Y.; Trout, B. L. Binding Affinity of a Small Molecule to an Amorphous Polymer in a Solvent. Part 1: Free Energy of Binding to a Binding Site. *Langmuir* **2011**, *27* (20), 12381−12395.
(40) Diao, Y.; Harada, T.; Myerson, A. S.; Alan Hatton, T.; Trout, B. L. The role of nanopore shape in surface-induced crystallization. *Nat. Mater.* **2011**, *10* (11), 867−871.
(41) Trout, B. L.; Doyle, P. S.; Hatton, T. A.; Myerson, A. S.; Diao, Y.; Helgeson, M. E. Compositions, methods, and systems relating to controlled crystallization and/or nucleation of molecular species. US20120076860A1, 2012.
(42) Sharma, M.; Trout, B. L. Effect of Pore Size and Interactions on Paracetamol Aggregation in Porous Polyethylene Glycol Diacrylate Polymers. *J. Phys. Chem. B* **2015**, *119* (25), 8135−8145.
(43) López-Mejías, V.; Knight, J. L.; Brooks, C. L.; Matzger, A. J. On the Mechanism of Crystalline Polymorph Selection by Polymer Heteronuclei. *Langmuir* **2011**, *27* (12), 7575−7579.
(44) Curcio, E.; López-Mejías, V.; Di Profio, G.; Fontananova, E.; Drioli, E.; Trout, B. L.; Myerson, A. S. Regulating Nucleation Kinetics through Molecular Interactions at the Polymer−Solute Interface. *Cryst. Growth Des.* **2014**, *14* (2), 678−686.
(45) López-Mejías, V.; Kampf, J. W.; Matzger, A. J. Polymer-Induced Heteronucleation of Tolfenamic Acid: Structural Investigation of a Pentamorph. *J. Am. Chem. Soc.* **2009**, *131* (13), 4554−4555.
(46) Evans, T.; Sarofim, A.; Margolis, G. Models of secondary nucleation attributable to crystal-crystallizer and crystal-crystal collisions. *AIChE J.* **1974**, *20* (5), 959−966.
(47) Ottens, E.; de Jong, E. A model for secondary nucleation in a stirred vessel cooling crystallizer. *Krist. Tech.* **1974**, *9* (8), 873−886.
(48) Liiri, M.; Koiranen, T.; Aittamaa, J. Secondary nucleation due to crystal−impeller and crystal−vessel collisions by population balances in CFD-modelling. *J. Cryst. Growth* **2002**, *237*−*239* (Part 3), 2188−2193.
(49) Rahimi, M.; Amraei, S.; Alsairafi, A. A. Experimental and computational fluid dynamics modeling of mixing by Visco-jet impellers. *Korean J. Chem. Eng.* **2011**, *28* (6), 1372−1379.
(50) Granberg, R. A.; Rasmuson, Å. C. Solubility of Paracetamol in Pure Solvents. *J. Chem. Eng. Data* **1999**, *44* (6), 1391−1395.
(51) Soare, A.; Lakerveld, R.; Van Royen, J.; Zocchi, G.; Stankiewicz, A. I.; Kramer, H. J. Minimization of attrition and breakage in an airlift crystallizer. *Ind. Eng. Chem. Res.* **2012**, *51* (33), 10895−10909.
(52) Lakerveld, R.; Van Krochten, J. J.; Kramer, H. J. An air-lift crystallizer can suppress secondary nucleation at a higher supersaturation compared to a stirred crystallizer. *Cryst. Growth Des.* **2014**, *14* (7), 3264−3275.
(53) Neumann, A. M.; Bermingham, S. K.; Kramer, H. J.; Van Rosmalen, G. M. Modeling the Attrition Process in a 22 Liter Draft Tube Crystallizer. In *Mixing and Crystallization*; Springer, 2000; pp 267−279.
(54) Fujiwara, M.; Chow, P. S.; Ma, D. L.; Braatz, R. D. Paracetamol crystallization using laser backscattering and ATR-FTIR spectroscopy: metastability, agglomeration, and control. *Cryst. Growth Des.* **2002**, *2* (5), 363−370.
(55) Zhu, Z.; Peng, Y.; Hatton, T. A.; Samrane, K.; Myerson, A. S.; Braatz, R. D. Crystallization of Calcium Sulphate During Phosphoric Acid Production: Modeling Particle Shape and Size Distribution. *Procedia Eng.* **2016**, *138*, 390−402.
(56) Yazdanpanah, N.; Myerson, A.; Trout, B. Mathematical Modeling of Layer Crystallization on a Cold Column with Recirculation. *Ind. Eng. Chem. Res.* **2016**, *55* (17), 5019−5029.
(57) Yazdanpanah, N.; Ferguson, S. T.; Myerson, A. S.; Trout, B. L. Novel Technique for Filtration Avoidance in Continuous Crystallization. *Cryst. Growth Des.* **2016**, *16* (1), 285−296.
(58) Rasenack, N.; Müller, B. W. Crystal habit and tableting behavior. *Int. J. Pharm.* **2002**, *244* (1), 45−57.
(59) Beretzky, Á.; Kása, P., Jr.; Pintye-Hódi, K.; Bajdik, J.; Szabó-Révész, P.; Erős, I. Pelletization of needle-shaped phenylbutazone crystals. *J. Therm. Anal. Calorim.* **2002**, *69* (2), 529−539.
(60) Perumalla, S. R.; Shi, L.; Sun, C. C. Ionized form of acetaminophen with improved compaction properties. *CrystEngComm* **2012**, *14* (7), 2389−2390.

DOI: 10.1021/acs.cgd.7b00297
Cryst. Growth Des. 2017, 17, 3321−3330